

Observation of $D^{0(+)} \rightarrow K_S^0 \pi^{0(+)} \omega$ and improved measurement of $D^0 \rightarrow K^- \pi^+ \omega$

M. Ablikim¹, M. N. Achasov^{10,c}, P. Adlarson⁶⁷, S. Ahmed¹⁵, M. Albrecht⁴, R. Aliberti²⁸, A. Amoroso^{66A,66C}, M. R. An³², Q. An^{63,49}, X. H. Bai⁵⁷, Y. Bai⁴⁸, O. Bakina²⁹, R. Baldini Ferroli^{23A}, I. Balossino^{24A}, Y. Ban^{38,k}, K. Begzsuren²⁶, N. Berger²⁸, M. Bertani^{23A}, D. Bettoni^{24A}, F. Bianchi^{66A,66C}, J. Bloms⁶⁰, A. Bortone^{66A,66C}, I. Boyko²⁹, R. A. Briere⁵, H. Cai⁶⁸, X. Cai^{1,49}, A. Calcaterra^{23A}, G. F. Cao^{1,54}, N. Cao^{1,54}, S. A. Cetin^{53A}, J. F. Chang^{1,49}, W. L. Chang^{1,54}, G. Chelkov^{29,b}, D. Y. Chen⁶, G. Chen¹, H. S. Chen^{1,54}, M. L. Chen^{1,49}, S. J. Chen³⁵, X. R. Chen²⁵, Y. B. Chen^{1,49}, Z. J. Chen^{20,l}, W. S. Cheng^{66C}, G. Cibinetto^{24A}, F. Cossio^{66C}, X. F. Cui³⁶, H. L. Dai^{1,49}, X. C. Dai^{1,54}, A. Dbeyssi¹⁵, R. E. de Boer⁴, D. Dedovich²⁹, Z. Y. Deng¹, A. Denig²⁸, I. Denysenko²⁹, M. Destefanis^{66A,66C}, F. De Mori^{66A,66C}, Y. Ding³³, C. Dong³⁶, J. Dong^{1,49}, L. Y. Dong^{1,54}, M. Y. Dong^{1,49,54}, X. Dong⁶⁸, S. X. Du⁷¹, Y. L. Fan⁶⁸, J. Fang^{1,49}, S. S. Fang^{1,54}, Y. Fang¹, R. Farinelli^{24A}, L. Fava^{66B,66C}, F. Feldbauer⁴, G. Felici^{23A}, C. Q. Feng^{63,49}, J. H. Feng⁵⁰, M. Fritsch⁴, C. D. Fu¹, Y. Gao^{38,k}, Y. Gao⁶⁴, Y. Gao^{63,49}, Y. G. Gao⁶, I. Garzia^{24A,24B}, P. T. Ge⁶⁸, C. Geng⁵⁰, E. M. Gersabeck⁵⁸, A. Gilman⁶¹, K. Goetzen¹¹, L. Gong³³, W. X. Gong^{1,49}, W. Gradl²⁸, M. Greco^{66A,66C}, L. M. Gu³⁵, M. H. Gu^{1,49}, S. Gu², Y. T. Gu¹³, C. Y. Guan^{1,54}, A. Q. Guo²², L. B. Guo³⁴, R. P. Guo⁴⁰, Y. P. Guo^{9,h}, Yupei Guo¹⁶, A. Guskov²⁹, T. T. Han⁴¹, W. Y. Han³², X. Q. Hao¹⁶, F. A. Harris⁵⁶, N. Hüskens^{22,28}, K. L. He^{1,54}, F. H. Heinsius⁴, C. H. Heinz²⁸, T. Held⁴, Y. K. Heng^{1,49,54}, C. Herold⁵¹, M. Himmelreich^{11,f}, T. Holtmann⁴, Y. R. Hou⁵⁴, Z. L. Hou¹, H. M. Hu^{1,54}, J. F. Hu^{47,m}, T. Hu^{1,49,54}, Y. Hu¹, G. S. Huang^{63,49}, L. Q. Huang⁶⁴, X. T. Huang⁴¹, Y. P. Huang¹, Z. Huang^{38,k}, T. Hussain⁶⁵, W. Ikegami Andersson⁶⁷, W. Imoehl²², M. Irshad^{63,49}, S. Jaeger⁴, S. Janchiv^{26,j}, Q. Ji¹, Q. P. Ji¹⁶, X. B. Ji^{1,54}, X. L. Ji^{1,49}, Y. Y. Ji⁴¹, H. B. Jiang⁴¹, X. S. Jiang^{1,49,54}, J. B. Jiao⁴¹, Z. Jiao¹⁸, S. Jin³⁵, Y. Jin⁵⁷, T. Johansson⁶⁷, N. Kalantar-Nayestanaki⁵⁵, X. S. Kang³³, R. Kappert⁵⁵, M. Kavatsyuk⁵⁵, B. C. Ke^{43,1}, I. K. Keshk⁴, A. Khokkaz⁶⁰, P. Kiese²⁸, R. Kiuchi¹, R. Kliemt¹¹, L. Koch³⁰, O. B. Kolcu^{53A,e}, B. Kopf⁴, M. Kuemmel⁴, M. Kuessner⁴, A. Kupsc⁶⁷, M. G. Kurth^{1,54}, W. Kühn³⁰, J. J. Lane⁵⁸, J. S. Lange³⁰, P. Larin¹⁵, A. Lavania²¹, L. Lavezzi^{66A,66C}, Z. H. Lei^{63,49}, H. Leithoff²⁸, M. Lellmann²⁸, T. Lenz²⁸, C. Li³⁹, C. H. Li³², Cheng Li^{63,49}, D. M. Li⁷¹, F. Li^{1,49}, G. Li¹, H. Li⁴³, H. Li^{63,49}, H. B. Li^{1,54}, H. J. Li¹⁶, J. L. Li⁴¹, J. Q. Li⁴, J. S. Li⁵⁰, Ke Li¹, L. K. Li¹, Lei Li³, P. R. Li³¹, S. Y. Li⁵², W. D. Li^{1,54}, W. G. Li¹, X. H. Li^{63,49}, X. L. Li⁴¹, Xiaoyu Li^{1,54}, Z. Y. Li⁵⁰, H. Liang^{1,54}, H. Liang^{63,49}, H. Liang²⁷, Y. F. Liang⁴⁵, Y. T. Liang²⁵, G. R. Liao¹², L. Z. Liao^{1,54}, J. Libby²¹, C. X. Lin⁵⁰, B. J. Liu¹, C. X. Liu¹, D. Liu^{15,63}, F. H. Liu⁴⁴, Fang Liu¹, Feng Liu⁶, H. B. Liu¹³, H. M. Liu^{1,54}, Huanhuan Liu¹, Huihui Liu¹⁷, J. B. Liu^{63,49}, J. L. Liu⁶⁴, J. Y. Liu^{1,54}, K. Liu¹, K. Y. Liu³³, L. Liu^{63,49}, M. H. Liu^{9,h}, P. L. Liu¹, Q. Liu⁵⁴, Q. Liu⁶⁸, S. B. Liu^{63,49}, Shuai Liu⁴⁶, T. Liu^{1,54}, W. M. Liu^{63,49}, X. Liu³¹, Y. Liu³¹, Y. B. Liu³⁶, Z. A. Liu^{1,49,54}, Z. Q. Liu⁴¹, X. C. Lou^{1,49,54}, F. X. Lu⁵⁰, H. J. Lu¹⁸, J. D. Lu^{1,54}, J. G. Lu^{1,49}, X. L. Lu¹, Y. Lu¹, Y. P. Lu^{1,49}, C. L. Luo³⁴, M. X. Luo⁷⁰, P. W. Luo⁵⁰, T. Luo^{9,h}, X. L. Luo^{1,49}, X. R. Lyu⁵⁴, F. C. Ma³³, H. L. Ma¹, L. L. Ma⁴¹, M. M. Ma^{1,54}, Q. M. Ma¹, R. Q. Ma^{1,54}, R. T. Ma⁵⁴, X. X. Ma^{1,54}, X. Y. Ma^{1,49}, F. E. Maas¹⁵, M. Maggiora^{66A,66C}, S. Maldaner⁴, S. Malde⁶¹, Q. A. Malik⁶⁵, A. Mangoni^{23B}, Y. J. Mao^{38,k}, Z. P. Mao¹, S. Marcello^{66A,66C}, Z. X. Meng⁵⁷, J. G. Messchendorp⁵⁵, G. Mezzadri^{24A}, T. J. Min³⁵, R. E. Mitchell²², X. H. Mo^{1,49,54}, Y. J. Mo⁶, N. Yu. Muchnoi^{10,c}, H. Muramatsu⁵⁹, S. Nakhoul^{11,f}, Y. Nefedov²⁹, F. Nerling^{11,f}, I. B. Nikolaev^{10,c}, Z. Ning^{1,49}, S. Nisar^{8,i}, S. L. Olsen⁵⁴, Q. Ouyang^{1,49,54}, S. Pacetti^{23B,23C}, X. Pan^{9,h}, Y. Pan⁵⁸, A. Pathak¹, P. Patteri^{23A}, M. Pelizaeus⁴, H. P. Peng^{63,49}, K. Peters^{11,f}, J. Pettersson⁶⁷, J. L. Ping³⁴, R. G. Ping^{1,54}, R. Poling⁵⁹, V. Prasad^{63,49}, H. Qi^{63,49}, H. R. Qi⁵², K. H. Qi²⁵, M. Qi³⁵, T. Y. Qi⁹, S. Qian^{1,49}, W. B. Qian⁵⁴, Z. Qian⁵⁰, C. F. Qiao⁵⁴, L. Q. Qin¹², X. P. Qin⁹, X. S. Qin⁴¹, Z. H. Qin^{1,49}, J. F. Qiu¹, S. Q. Qu³⁶, K. H. Rashid⁶⁵, K. Ravindran²¹, C. F. Redmer²⁸, A. Rivetti^{66C}, V. Rodin⁵⁵, M. Rolo^{66C}, G. Rong^{1,54}, Ch. Rosner¹⁵, M. Rump⁶⁰, H. S. Sang⁶³, A. Sarantsev^{29,d}, Y. Schelhaas²⁸, C. Schnier⁴, K. Schoenning⁶⁷, M. Scodeggio^{24A,24B}, D. C. Shan⁴⁶, W. Shan¹⁹, X. Y. Shan^{63,49}, J. F. Shanguan⁴⁶, M. Shao^{63,49}, C. P. Shen⁹, P. X. Shen³⁶, X. Y. Shen^{1,54}, H. C. Shi^{63,49}, R. S. Shi^{1,54}, X. Shi^{1,49}, X. D. Shi^{63,49}, J. J. Song⁴¹, W. M. Song^{27,1}, Y. X. Song^{38,k}, S. Sosio^{66A,66C}, S. Spataro^{66A,66C}, K. X. Su⁶⁸, P. P. Su⁴⁶, F. F. Sui⁴¹, G. X. Sun¹, H. K. Sun¹, J. F. Sun¹⁶, L. Sun⁶⁸, S. S. Sun^{1,54}, T. Sun^{1,54}, W. Y. Sun³⁴, W. Y. Sun²⁷, X. Sun^{20,l}, Y. J. Sun^{63,49}, Y. K. Sun^{63,49}, Y. Z. Sun¹, Z. T. Sun¹, Y. H. Tan⁶⁸, Y. X. Tan^{63,49}, C. J. Tang⁴⁵, G. Y. Tang¹, J. Tang⁵⁰, J. X. Teng^{63,49}, V. Thoren⁶⁷, W. H. Tian⁴³, Y. T. Tian²⁵, I. Uman^{53B}, B. Wang¹, C. W. Wang³⁵, D. Y. Wang^{38,k}, H. J. Wang³¹, H. P. Wang^{1,54}, K. Wang^{1,49}, L. L. Wang¹, M. Wang⁴¹, M. Z. Wang^{38,k}, Meng Wang^{1,54}, W. Wang⁵⁰, W. H. Wang⁶⁸, W. P. Wang^{63,49}, X. Wang^{38,k}, X. F. Wang³¹, X. L. Wang^{9,h}, Y. Wang^{63,49}, Y. Wang⁵⁰, Y. D. Wang³⁷, Y. F. Wang^{1,49,54}, Y. Q. Wang¹, Y. Y. Wang³¹, Z. Wang^{1,49}, Z. Y. Wang¹, Ziyi Wang⁵⁴, Zongyuan Wang^{1,54}, D. H. Wei¹², F. Weidner⁶⁰, S. P. Wen¹, D. J. White⁵⁸, U. Wiedner⁴, G. Wilkinson⁶¹, M. Wolke⁶⁷, L. Wollenberg⁴, J. F. Wu^{1,54}, L. H. Wu¹, L. J. Wu^{1,54}, X. Wu^{9,h}, Z. Wu^{1,49}, L. Xia^{63,49}, H. Xiao^{9,h}, S. Y. Xiao¹, Z. J. Xiao³⁴, X. H. Xie^{38,k}, Y. G. Xie^{1,49}, Y. H. Xie⁶, T. Y. Xing^{1,54}, G. F. Xu¹,

Q. J. Xu¹⁴, W. Xu^{1,54}, X. P. Xu⁴⁶, Y. C. Xu⁵⁴, F. Yan^{9,h}, L. Yan^{9,h}, W. B. Yan^{63,49}, W. C. Yan⁷¹, Xu Yan⁴⁶,
H. J. Yang^{42,g}, H. X. Yang¹, L. Yang⁴³, S. L. Yang⁵⁴, Y. X. Yang¹², Yifan Yang^{1,54}, Zhi Yang²⁵, M. Ye^{1,49},
M. H. Ye⁷, J. H. Yin¹, Z. Y. You⁵⁰, B. X. Yu^{1,49,54}, C. X. Yu³⁶, G. Yu^{1,54}, J. S. Yu^{20,l}, T. Yu⁶⁴, C. Z. Yuan^{1,54},
L. Yuan², X. Q. Yuan^{38,k}, Y. Yuan¹, Z. Y. Yuan⁵⁰, C. X. Yue³², A. Yuncu^{53A,a}, A. A. Zafar⁶⁵, Zeng⁶, Y. Zeng^{20,l},
B. X. Zhang¹, Guangyi Zhang¹⁶, H. Zhang⁶³, H. H. Zhang⁵⁰, H. H. Zhang²⁷, H. Y. Zhang^{1,49}, J. J. Zhang⁴³,
J. L. Zhang⁶⁹, J. Q. Zhang³⁴, J. W. Zhang^{1,49,54}, J. Y. Zhang¹, J. Z. Zhang^{1,54}, Jianyu Zhang^{1,54}, Jiawei Zhang^{1,54},
L. M. Zhang⁵², L. Q. Zhang⁵⁰, Lei Zhang³⁵, S. Zhang⁵⁰, S. F. Zhang³⁵, Shulei Zhang^{20,l}, X. D. Zhang³⁷,
X. Y. Zhang⁴¹, Y. Zhang⁶¹, Y. H. Zhang^{1,49}, Y. T. Zhang^{63,49}, Yan Zhang^{63,49}, Yao Zhang¹, Yi Zhang^{9,h},
Z. H. Zhang⁶, Z. Y. Zhang⁶⁸, G. Zhao¹, J. Zhao³², J. Y. Zhao^{1,54}, J. Z. Zhao^{1,49}, Lei Zhao^{63,49}, Ling Zhao¹,
M. G. Zhao³⁶, Q. Zhao¹, S. J. Zhao⁷¹, Y. B. Zhao^{1,49}, Y. X. Zhao²⁵, Z. G. Zhao^{63,49}, A. Zhemchugov^{29,b},
B. Zheng⁶⁴, J. P. Zheng^{1,49}, Y. Zheng^{38,k}, Y. H. Zheng⁵⁴, B. Zhong³⁴, C. Zhong⁶⁴, L. P. Zhou^{1,54}, Q. Zhou^{1,54},
X. Zhou⁶⁸, X. K. Zhou⁵⁴, X. R. Zhou^{63,49}, X. Y. Zhou³², A. N. Zhu^{1,54}, J. Zhu³⁶, K. Zhu¹, K. J. Zhu^{1,49,54},
S. H. Zhu⁶², T. J. Zhu⁶⁹, W. J. Zhu^{9,h}, W. J. Zhu³⁶, Y. C. Zhu^{63,49}, Z. A. Zhu^{1,54}, B. S. Zou¹, J. H. Zou¹

(BESIII Collaboration)

¹ *Institute of High Energy Physics, Beijing 100049, People's Republic of China*

² *Beihang University, Beijing 100191, People's Republic of China*

³ *Beijing Institute of Petrochemical Technology, Beijing 102617, People's Republic of China*

⁴ *Bochum Ruhr-University, D-44780 Bochum, Germany*

⁵ *Carnegie Mellon University, Pittsburgh, Pennsylvania 15213, USA*

⁶ *Central China Normal University, Wuhan 430079, People's Republic of China*

⁷ *China Center of Advanced Science and Technology, Beijing 100190, People's Republic of China*

⁸ *COMSATS University Islamabad, Lahore Campus, Defence Road, Off Raiwind Road, 54000 Lahore, Pakistan*

⁹ *Fudan University, Shanghai 200443, People's Republic of China*

¹⁰ *G.I. Budker Institute of Nuclear Physics SB RAS (BINP), Novosibirsk 630090, Russia*

¹¹ *GSI Helmholtzcentre for Heavy Ion Research GmbH, D-64291 Darmstadt, Germany*

¹² *Guangxi Normal University, Guilin 541004, People's Republic of China*

¹³ *Guangxi University, Nanning 530004, People's Republic of China*

¹⁴ *Hangzhou Normal University, Hangzhou 310036, People's Republic of China*

¹⁵ *Helmholtz Institute Mainz, Staudinger Weg 18, D-55099 Mainz, Germany*

¹⁶ *Henan Normal University, Xinxiang 453007, People's Republic of China*

¹⁷ *Henan University of Science and Technology, Luoyang 471003, People's Republic of China*

¹⁸ *Huangshan College, Huangshan 245000, People's Republic of China*

¹⁹ *Hunan Normal University, Changsha 410081, People's Republic of China*

²⁰ *Hunan University, Changsha 410082, People's Republic of China*

²¹ *Indian Institute of Technology Madras, Chennai 600036, India*

²² *Indiana University, Bloomington, Indiana 47405, USA*

²³ *INFN Laboratori Nazionali di Frascati, (A)INFN Laboratori Nazionali di Frascati, I-00044, Frascati, Italy; (B)INFN Sezione di Perugia, I-06100, Perugia, Italy; (C)University of Perugia, I-06100, Perugia, Italy*

²⁴ *INFN Sezione di Ferrara, (A)INFN Sezione di Ferrara, I-44122, Ferrara, Italy; (B)University of Ferrara, I-44122, Ferrara, Italy*

²⁵ *Institute of Modern Physics, Lanzhou 730000, People's Republic of China*

²⁶ *Institute of Physics and Technology, Peace Ave. 54B, Ulaanbaatar 13330, Mongolia*

²⁷ *Jilin University, Changchun 130012, People's Republic of China*

²⁸ *Johannes Gutenberg University of Mainz, Johann-Joachim-Becher-Weg 45, D-55099 Mainz, Germany*

²⁹ *Joint Institute for Nuclear Research, 141980 Dubna, Moscow region, Russia*

³⁰ *Justus-Liebig-Universitaet Giessen, II. Physikalisches Institut, Heinrich-Buff-Ring 16, D-35392 Giessen, Germany*

³¹ *Lanzhou University, Lanzhou 730000, People's Republic of China*

³² *Liaoning Normal University, Dalian 116029, People's Republic of China*

³³ *Liaoning University, Shenyang 110036, People's Republic of China*

³⁴ *Nanjing Normal University, Nanjing 210023, People's Republic of China*

³⁵ *Nanjing University, Nanjing 210093, People's Republic of China*

³⁶ *Nankai University, Tianjin 300071, People's Republic of China*

³⁷ *North China Electric Power University, Beijing 102206, People's Republic of China*

- ³⁸ Peking University, Beijing 100871, People's Republic of China
- ³⁹ Qufu Normal University, Qufu 273165, People's Republic of China
- ⁴⁰ Shandong Normal University, Jinan 250014, People's Republic of China
- ⁴¹ Shandong University, Jinan 250100, People's Republic of China
- ⁴² Shanghai Jiao Tong University, Shanghai 200240, People's Republic of China
- ⁴³ Shanxi Normal University, Linfen 041004, People's Republic of China
- ⁴⁴ Shanxi University, Taiyuan 030006, People's Republic of China
- ⁴⁵ Sichuan University, Chengdu 610064, People's Republic of China
- ⁴⁶ Soochow University, Suzhou 215006, People's Republic of China
- ⁴⁷ South China Normal University, Guangzhou 510006, People's Republic of China
- ⁴⁸ Southeast University, Nanjing 211100, People's Republic of China
- ⁴⁹ State Key Laboratory of Particle Detection and Electronics,
Beijing 100049, Hefei 230026, People's Republic of China
- ⁵⁰ Sun Yat-Sen University, Guangzhou 510275, People's Republic of China
- ⁵¹ Suranaree University of Technology, University Avenue 111, Nakhon Ratchasima 30000, Thailand
- ⁵² Tsinghua University, Beijing 100084, People's Republic of China
- ⁵³ Turkish Accelerator Center Particle Factory Group, (A)Istanbul Bilgi University, 34060 Eyup, Istanbul, Turkey; (B)Near East University, Nicosia, North Cyprus, Mersin 10, Turkey
- ⁵⁴ University of Chinese Academy of Sciences, Beijing 100049, People's Republic of China
- ⁵⁵ University of Groningen, NL-9747 AA Groningen, The Netherlands
- ⁵⁶ University of Hawaii, Honolulu, Hawaii 96822, USA
- ⁵⁷ University of Jinan, Jinan 250022, People's Republic of China
- ⁵⁸ University of Manchester, Oxford Road, Manchester, M13 9PL, United Kingdom
- ⁵⁹ University of Minnesota, Minneapolis, Minnesota 55455, USA
- ⁶⁰ University of Muenster, Wilhelm-Klemm-Str. 9, 48149 Muenster, Germany
- ⁶¹ University of Oxford, Keble Rd, Oxford, UK OX13RH
- ⁶² University of Science and Technology Liaoning, Anshan 114051, People's Republic of China
- ⁶³ University of Science and Technology of China, Hefei 230026, People's Republic of China
- ⁶⁴ University of South China, Hengyang 421001, People's Republic of China
- ⁶⁵ University of the Punjab, Lahore-54590, Pakistan
- ⁶⁶ University of Turin and INFN, (A)University of Turin, I-10125, Turin, Italy; (B)University of Eastern Piedmont, I-15121, Alessandria, Italy; (C)INFN, I-10125, Turin, Italy
- ⁶⁷ Uppsala University, Box 516, SE-75120 Uppsala, Sweden
- ⁶⁸ Wuhan University, Wuhan 430072, People's Republic of China
- ⁶⁹ Xinyang Normal University, Xinyang 464000, People's Republic of China
- ⁷⁰ Zhejiang University, Hangzhou 310027, People's Republic of China
- ⁷¹ Zhengzhou University, Zhengzhou 450001, People's Republic of China
- ^a Also at Bogazici University, 34342 Istanbul, Turkey
- ^b Also at the Moscow Institute of Physics and Technology, Moscow 141700, Russia
- ^c Also at the Novosibirsk State University, Novosibirsk, 630090, Russia
- ^d Also at the NRC "Kurchatov Institute", PNPI, 188300, Gatchina, Russia
- ^e Also at Istanbul Arel University, 34295 Istanbul, Turkey
- ^f Also at Goethe University Frankfurt, 60323 Frankfurt am Main, Germany
- ^g Also at Key Laboratory for Particle Physics, Astrophysics and Cosmology, Ministry of Education; Shanghai Key Laboratory for Particle Physics and Cosmology; Institute of Nuclear and Particle Physics, Shanghai 200240, People's Republic of China
- ^h Also at Key Laboratory of Nuclear Physics and Ion-beam Application (MOE) and Institute of Modern Physics, Fudan University, Shanghai 200443, People's Republic of China
- ⁱ Also at Harvard University, Department of Physics, Cambridge, MA, 02138, USA
- ^j Currently at: Institute of Physics and Technology, Peace Ave.54B, Ulaanbaatar 13330, Mongolia
- ^k Also at State Key Laboratory of Nuclear Physics and Technology,
Peking University, Beijing 100871, People's Republic of China
- ^l School of Physics and Electronics, Hunan University, Changsha 410082, China

^m Also at Guangdong Provincial Key Laboratory of Nuclear Science, Institute of Quantum Matter, South China Normal University, Guangzhou 510006, China

By analyzing an e^+e^- annihilation data sample with an integrated luminosity of 2.93 fb^{-1} taken at the center-of-mass energy of 3.773 GeV with the BESIII detector, we determine the absolute branching fractions of the hadronic decays $D^0 \rightarrow K^-\pi^+\omega$, $D^0 \rightarrow K_S^0\pi^0\omega$, and $D^+ \rightarrow K_S^0\pi^+\omega$ to be $(3.392 \pm 0.044_{\text{stat}} \pm 0.085_{\text{syst}})\%$, $(0.848 \pm 0.046_{\text{stat}} \pm 0.031_{\text{syst}})\%$, and $(0.707 \pm 0.041_{\text{stat}} \pm 0.029_{\text{syst}})\%$, respectively. The accuracy of the branching fraction measurement of the decay $D^0 \rightarrow K^-\pi^+\omega$ is improved by a factor of seven compared to the world average value. The $D^0 \rightarrow K_S^0\pi^0\omega$ and $D^+ \rightarrow K_S^0\pi^+\omega$ decays are observed for the first time.

PACS numbers: 13.20.Fc, 14.40.Lb

I. INTRODUCTION

Experimental studies of hadronic $D^{0(+)}$ decays can be used to investigate charm mixing, CP violation, and strong-interaction effects [1, 2]. Since the discoveries of the $D^{0(+)}$, hadronic $D^{0(+)}$ decays have been intensively studied [3]. However, while the branching fraction of the decay $D^0 \rightarrow K^-\pi^+\omega$ has previously been measured by the ARGUS Collaboration to be $(3.0 \pm 0.6)\%$ [3, 4], there are no measurements of the decays $D^0 \rightarrow K_S^0\pi^0\omega$ and $D^+ \rightarrow K_S^0\pi^+\omega$. According to the statistical isospin model (SIM) [5, 6], the branching fractions for these isospin multiplets are expected to satisfy $\mathcal{R}^0 \equiv \frac{\mathcal{B}(D^0 \rightarrow K_S^0\pi^0\omega)}{\mathcal{B}(D^0 \rightarrow K^-\pi^+\omega)} = 0.4$ and $\mathcal{R}^+ \equiv \frac{\mathcal{B}(D^+ \rightarrow K_S^0\pi^+\omega)}{\mathcal{B}(D^0 \rightarrow K^-\pi^+\omega)} = 0.9$. Measurements of the branching fractions of these three decays can be used to test this relation. In addition, these branching fractions provide important input for the background estimations needed to precisely test lepton flavor universality in semileptonic B decays [7] and to restrict new physics in the $D \rightarrow \bar{K}\pi\ell^+\ell^-$ decay [8–10].

In this paper, we report an improved measurement of the branching fraction of $D^0 \rightarrow K^-\pi^+\omega$, and also report the first observations and branching fraction measurements of the decays $D^0 \rightarrow K_S^0\pi^0\omega$ and $D^+ \rightarrow K_S^0\pi^+\omega$. This analysis is performed by using an e^+e^- collision data sample corresponding to an integrated luminosity of 2.93 fb^{-1} [11] collected at a center-of-mass energy of $\sqrt{s} = 3.773 \text{ GeV}$ with the BESIII detector. Throughout this paper, charge-conjugated modes are implied.

II. BESIII DETECTOR AND MONTE CARLO SIMULATION

The BESIII detector is a magnetic spectrometer [12] located at the Beijing Electron Positron Collider (BEPCII) [13]. The cylindrical core of the BESIII detector consists of a helium-based multilayer drift chamber (MDC), a plastic scintillator time-of-flight system (TOF), and a CsI(Tl) electromagnetic calorimeter (EMC), which are all enclosed in a superconducting solenoidal magnet providing a 1.0 T magnetic field. The

solenoid is supported by an octagonal flux-return yoke with resistive plate modules interleaved with steel that provides muon identification. The acceptance of charged particles and photons is 93% of the solid angle. The charged-particle momentum resolution at 1 GeV/c is 0.5%, and the dE/dx resolution is 6% for the electrons from Bhabha scattering. The EMC measures photon energies with a resolution of 2.5% (5%) at 1 GeV in the barrel (end cap) region. The time resolution of the TOF barrel region is 68 ps, while that of the end cap region is 110 ps. The effect of the trigger efficiency is negligible in this analysis according to Refs. [14, 15].

Simulated data samples produced with a GEANT4-based [16] Monte Carlo (MC) package, which includes the geometric description of the BESIII detector and the detector response, are used to determine detection efficiencies and estimate backgrounds. The simulation models the beam energy spread and initial state radiation (ISR) in the e^+e^- annihilations with the generator KKMC [17]. The inclusive MC samples include the production of $D\bar{D}$ pairs (including quantum coherence for the neutral D channels), the non- $D\bar{D}$ decays of the $\psi(3770)$, the ISR production of the J/ψ and $\psi(3686)$ states, and the continuum processes. The known decay modes are modeled with EVTGEN [18] using branching fractions taken from the Particle Data Group (PDG) [3], and the remaining unknown charmonium decays are modeled with LUNDCHARM [19]. Final state radiation from charged final state particles is incorporated using the PHOTOS package [20].

III. DOUBLE-TAG METHOD

At $\sqrt{s} = 3.773 \text{ GeV}$, the $\psi(3770)$ resonance is produced in e^+e^- annihilation and decays predominantly into $D^0\bar{D}^0$ or D^+D^- pairs, without additional particles in the final state. This property allows us to determine absolute branching fractions of D decays with a double-tag method [21]. In this method, the single-tag candidates are selected by reconstructing a \bar{D}^0 or D^- in the following hadronic final states: $\bar{D}^0 \rightarrow K^+\pi^-$, $K^+\pi^-\pi^0$, and $K^+\pi^-\pi^-\pi^+$, and $D^- \rightarrow K^+\pi^-\pi^-$, $K_S^0\pi^-$, $K^+\pi^-\pi^-\pi^0$, $K_S^0\pi^-\pi^0$, $K_S^0\pi^+\pi^-\pi^-$, and $K^+K^-\pi^-$. The events in which a signal candidate

can be reconstructed from the particles recoiling against the single-tag \bar{D} meson are called double-tag events. The branching fraction for the signal decay is determined by

$$\mathcal{B}_{\text{sig}} = N_{\text{DT}}^{\text{tot}} / (N_{\text{ST}}^{\text{tot}} \epsilon_{\text{sig}}), \quad (1)$$

where $N_{\text{ST}}^{\text{tot}} = \sum_i N_{\text{tag}}^i$ and $N_{\text{DT}}^{\text{tot}}$ represent the total single-tag yield and the double-tag yield, respectively; and ϵ_{sig} is the efficiency of detecting the signal decay in the presence of a single-tag D meson, averaged over all tag modes

$$\epsilon_{\text{sig}} = \sum_i (N_{\text{tag}}^i \epsilon_{\text{sig}}^i) / N_{\text{ST}}^{\text{tot}}. \quad (2)$$

Here, $\epsilon_{\text{sig}}^i = \epsilon_{\text{tag, sig}}^i / \epsilon_{\text{tag}}^i$, where ϵ_{tag}^i and $\epsilon_{\text{tag, sig}}^i$ are the efficiencies of reconstructing the single-tag candidates and the double-tag events, respectively.

IV. EVENT SELECTION

We use the same selection criteria for K^\pm , π^\pm , K_S^0 , γ and π^0 as were used in Refs. [22–32]. The polar angle of each charged track is required to satisfy $|\cos\theta| < 0.93$. Except for those tracks used to reconstruct K_S^0 mesons, their minimum distances to the interaction point (IP) are required to be within 10 cm in the beam direction and within 1 cm in the perpendicular plane. The particle identification (PID) of each charged track is determined using dE/dx and TOF information. The combined confidence levels for kaon and pion hypotheses are calculated, and denoted as CL_K and CL_π . A charged track is identified as a kaon candidate if CL_K is greater than CL_π , or as a pion candidate if CL_π is greater than CL_K .

The K_S^0 candidates are obtained from two pions with opposite charges. For the two charged pions, the requirement on the closest approach to the IP in the beam direction is required to be within 20 cm, and no requirements on the distance in the perpendicular plane and on PID are imposed. The two charged pions are constrained to originate from a common vertex at the IP, and must have an invariant mass $M_{\pi^+\pi^-}$ within $\pm 12 \text{ MeV}/c^2$ of the nominal mass of the K_S^0 [3]. For a K_S^0 candidate, the measured flight distance away from the IP is required to be greater than twice its uncertainty. Figure 1(a) shows the $M_{\pi^+\pi^-}$ distribution of K_S^0 candidates, where two solid arrows denote the K_S^0 signal region.

Photon candidates are chosen from isolated EMC clusters with energies greater than 25 (50) MeV, if the crystal with the maximum deposited energy in that cluster is in the barrel (end cap) region [12]. To reject photons from bremsstrahlung or from interactions with material, showers within a 10° cone around the momentum direction of any charged track are rejected. Reconstructed showers due to electronic noise or beam

backgrounds are suppressed by requiring the timing information to be within $[0, 700] \text{ ns}$ after the event start time. The π^0 candidates are reconstructed from photon pairs. To form a π^0 candidate, the invariant mass of the photon pair is required to be in the interval $(0.115, 0.150) \text{ GeV}/c^2$. A one-constraint (1-C) kinematic fit is imposed on the photon pair to improve the momentum resolution. In the kinematic fit, the invariant mass of the photon pair is constrained at the nominal mass of the π^0 [3].

In the selection of $\bar{D}^0 \rightarrow K^+\pi^-$ tags, the backgrounds from cosmic rays and Bhabha events are suppressed by employing the following requirements. First, the two charged tracks must have a TOF time difference less than 5 ns, and they must not be consistent with being a muon pair or an electron-positron pair. Second, there must be at least one EMC shower with an energy larger than 50 MeV or at least one additional charged track detected in the MDC [33]. In the selection of $\bar{D}^0 \rightarrow K^+\pi^-\pi^-\pi^+$ candidates, the $\bar{D}^0 \rightarrow K_S^0 K^\pm \pi^\mp$ decays are suppressed by requiring the mass of all $\pi^+\pi^-$ pairs to be outside of $(0.478, 0.518) \text{ GeV}/c^2$.

To distinguish the tagged \bar{D} (signal D) mesons from combinatorial backgrounds, their energy difference and beam-constrained mass are defined as

$$\Delta E^{\text{tag (sig)}} \equiv E_{\bar{D}(D)} - E_b, \quad (3)$$

$$M_{\text{BC}}^{\text{tag (sig)}} \equiv \sqrt{E_b^2/c^4 - |\vec{p}_{\bar{D}(D)}|^2/c^2}, \quad (4)$$

where tag and sig denote tag and signal sides, respectively; E_b is the beam energy; and $\vec{p}_{\bar{D}(D)}$ and $E_{\bar{D}(D)}$ are the momentum and energy of the $\bar{D}(D)$ candidate in the rest frame of the e^+e^- system. For each tag (signal) mode, if multiple candidates are present, the one with the smallest $|\Delta E^{\text{tag (sig)}}|$ is kept for further analysis. The ΔE^{tag} is required to be in the range $(-55, +40) \text{ MeV}$ for the tag modes containing π^0 and within $(-25, +25) \text{ MeV}$ for the other modes. The ΔE^{sig} is required to be in the range $(-34, +41) \text{ MeV}$, $(-42, +57) \text{ MeV}$, and $(-37, +44) \text{ MeV}$ for $D^0 \rightarrow K^-\pi^+\omega$, $D^0 \rightarrow K_S^0\pi^0\omega$, and $D^+ \rightarrow K_S^0\pi^+\omega$, respectively. These requirements correspond to about 3.5 times the fitted mass resolutions away from the fitted peaks. They are different for various modes to take different resolutions into account. The requirements for the modes containing π^0 in the final state are asymmetric mainly due to photon energy losses before entering the EMC.

The ω candidates are selected from the $\pi^+\pi^-\pi^0$ combinations with an invariant mass $M_{\pi^+\pi^-\pi^0}$ within $\pm 25 \text{ MeV}/c^2$ of the nominal ω mass [3]. Figure 1(b) shows the $M_{\pi^+\pi^-\pi^0}$ distribution of ω candidates, where two solid arrows denote the ω signal region. The $D^0 \rightarrow K^-\pi^+\omega$, $D^0 \rightarrow K_S^0\pi^0\omega$ and $D^+ \rightarrow K_S^0\pi^+\omega$ decays are selected from the $K^-\pi^+\pi^+\pi^-\pi^0$, $K_S^0\pi^+\pi^+\pi^-\pi^0$ and $K_S^0\pi^+\pi^0\pi^-\pi^0$ final states. As a result, there

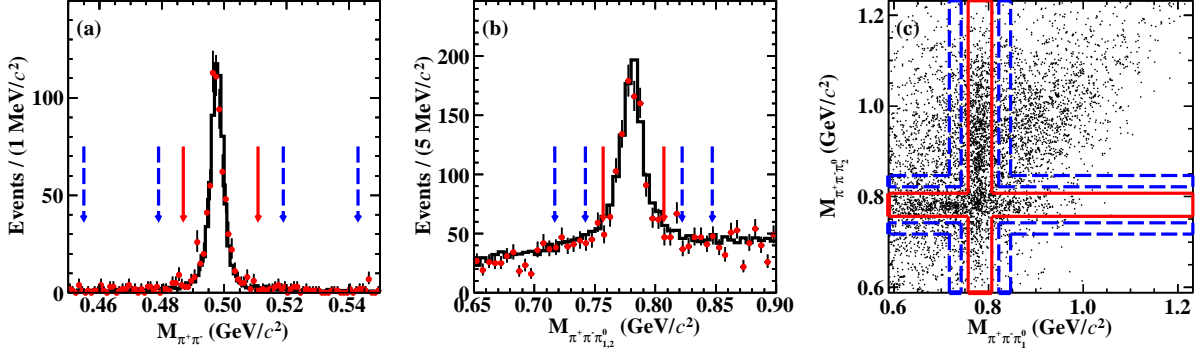


Fig. 1. (a) The $M_{\pi^+\pi^-}$ distribution of the K_S^0 candidates, (b) the combined $M_{\pi^+\pi^-\pi_1^0}$ and $M_{\pi^+\pi^-\pi_2^0}$ distribution of the ω candidates, and (c) the distribution of $M_{\pi^+\pi^-\pi_1^0}$ versus $M_{\pi^+\pi^-\pi_2^0}$ from the $D^0 \rightarrow K_S^0 \pi^0 \omega$ candidate events in data. The red solid (blue dashed) arrows [lines] show the corresponding boundaries of the 1D (2D) signal (sideband) region. In these figures, except for the K_S^0 or ω mass requirement, all other selection criteria and additional requirements of $|M_{\text{BC}}^{\text{tag}(\text{sig})} - M_D| < 0.005$ GeV/c² have been imposed. The signal and sideband regions, illustrated here, are applied to all decays used in these analysis. In plots (a) and (b), points with error bars are data and histograms are the inclusive MC sample.

are two possible $\pi^+\pi^-\pi^0$ combinations when selecting the ω candidate. Their invariant masses are denoted as $M_{\pi_1^+\pi^-\pi^0}$ and $M_{\pi_2^+\pi^-\pi^0}$ for $K\pi^+\pi^+\pi^-\pi^0$. Their invariant masses are denoted as $M_{\pi^+\pi^-\pi_1^0}$ and $M_{\pi^+\pi^-\pi_2^0}$ for $K_S^0\pi^+\pi^-\pi^0\pi^0$, respectively. Figure 1(c) shows the distribution of $M_{\pi_2^+\pi^-\pi^0}$ versus $M_{\pi_1^+\pi^-\pi^0}$ for the accepted candidate events from the $D^0 \rightarrow K^-\pi^+\omega$ decay in data. Events in the two dimensional (2D) ω signal region, as outlined by the red lines in Fig. 1(c), are kept for further analysis.

V. SINGLE-TAG AND DOUBLE-TAG YIELDS

The $M_{\text{BC}}^{\text{tag}}$ distributions of the accepted single-tag candidates in data are shown in Fig. 2. To determine the single-tag yield for each tag mode, a maximum likelihood fit is performed on the corresponding $M_{\text{BC}}^{\text{tag}}$ spectrum. An MC-simulated shape convolved with a double Gaussian function is used to model the \bar{D} signal. The convolved double Gaussian function describes the difference between the resolution in data and in MC simulation. The combinatorial background shape is described by an ARGUS function [34] defined as $c_f(f; E_{\text{end}}, \xi_f) = A_f \cdot f \cdot \sqrt{1 - \frac{f^2}{E_{\text{end}}^2}} \cdot \exp\left[\xi_f \left(1 - \frac{f^2}{E_{\text{end}}^2}\right)\right]$, where f denotes $M_{\text{BC}}^{\text{tag}}$, E_{end} is an endpoint fixed at 1.8865 GeV, A_f is a normalization factor, and ξ_f is a free parameter. Figure 2 shows the fit results on the $M_{\text{BC}}^{\text{tag}}$ distributions. Finally, we obtain 1558163 ± 2113 single-tag D^- mesons and 2386554 ± 1928 single-tag \bar{D}^0 mesons, denoted as $N_{\text{ST}}^{\text{tot}}$, where the uncertainties are statistical only.

Figure 3 illustrates the distribution of $M_{\text{BC}}^{\text{tag}}$ versus $M_{\text{BC}}^{\text{sig}}$ for double-tag candidate events. Signal events concentrate around $M_{\text{BC}}^{\text{tag}} = M_{\text{BC}}^{\text{sig}} = M_D$, where M_D

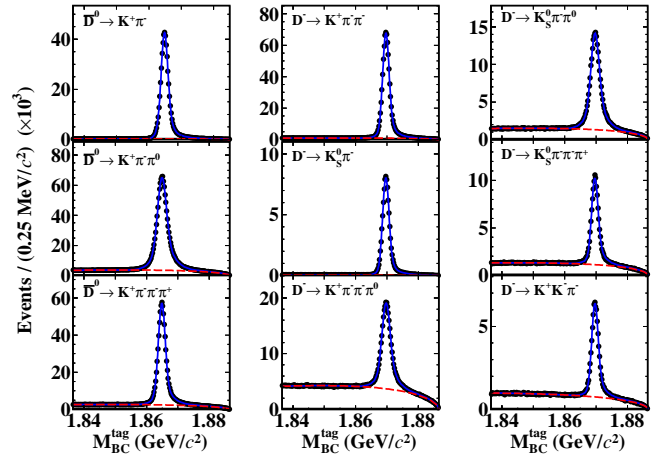


Fig. 2. Fits to the $M_{\text{BC}}^{\text{tag}}$ distributions of the single-tag \bar{D}^0 (left column) and D^- (middle and right columns) modes. Data are shown as points with error bars. The blue solid and red dashed curves are the fit results and the fitted background shapes, respectively.

is the nominal D mass [3]. Background events are divided into three categories. The first one (named BKGI) is from events with correctly reconstructed D (\bar{D}) and incorrectly reconstructed \bar{D} (D), which are spread along the lines around $M_{\text{BC}}^{\text{tag}}$ or $M_{\text{BC}}^{\text{sig}} = M_D$. The second one (named BKGII) is from events smeared along the diagonal, which are mainly from the $e^+e^- \rightarrow q\bar{q}$ processes. The events with uncorrelated and incorrectly reconstructed D and \bar{D} (named BKGIII) disperse across the whole allowed kinematic region. To extract the double-tag yield in data, we perform a two-dimensional (2D) unbinned maximum likelihood fit [35] on the underlying events. In the fit, the probability density functions (PDFs) of the signal, BKGI, BKGII, and

BKGIII are constructed as

- signal: $a(x, y)$,
- BKG I: $b(x) \cdot c_y(y; E_b, \xi_y) + b(y) \cdot c_x(x; E_b, \xi_x)$,
- BKG II: $c_z(z; \sqrt{2}E_b, \xi_z) \cdot g(k)$, and
- BKG III: $c_x(x; E_b, \xi_x) \cdot c_y(y; E_b, \xi_y)$,

respectively. Here, $x = M_{BC}^{\text{sig}}$, $y = M_{BC}^{\text{tag}}$, $z = (x + y)/\sqrt{2}$, and $k = (x - y)/\sqrt{2}$. The PDFs of signal $a(x, y)$, $b(x)$, and $b(y)$ are described by the corresponding MC-simulated shapes. In addition, $c_f(f; E_{\text{end}}, \xi_f)$ is an ARGUS function [34] (as defined above), where f denotes x , y , or z , and E_b is fixed at 1.8865 GeV; and $g(k)$ is a Gaussian function with a mean of zero and a standard deviation parametrized by $\sigma_k = \sigma_0 \cdot (\sqrt{2}E_b/c^2 - z)^p$, where σ_0 and p are fit parameters. For x and y , $E_{\text{end}} = E_b$, while $E_{\text{end}} = \sqrt{2}E_b$ for z .

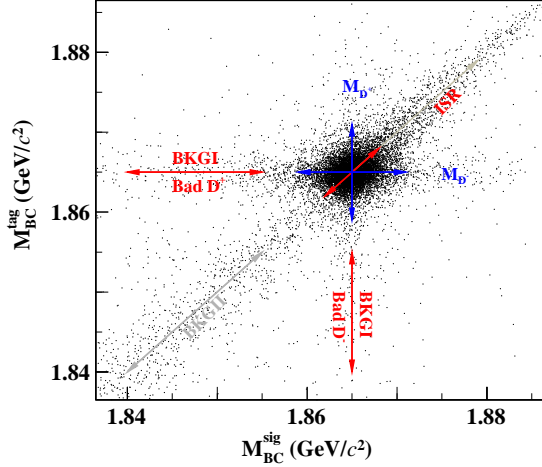


Fig. 3. The distribution of M_{BC}^{tag} versus M_{BC}^{sig} of the accepted double-tag $D\bar{D}$ candidate events for \bar{D}^0 tags versus $D^0 \rightarrow K^-\pi^+\omega$.

Projections on M_{BC}^{tag} and M_{BC}^{sig} of the 2D fits to the accepted double-tag candidate events are shown in Fig. 4. The second column of Table 1 presents the double-tag yields for individual signal decays ($N_{\text{DT}}^{\text{tot}}$).

Potential peaking backgrounds are investigated as follows. The combinatorial $\pi^+\pi^-$ pairs from the decays $D^0 \rightarrow K^-\pi^+\pi^+\pi^-\pi^0$, $D^0 \rightarrow K_S^0\pi^+\pi^-\pi^0\pi^0$ and $D^+ \rightarrow K_S^0\pi^+\pi^+\pi^-\pi^0$ or $\pi^+\pi^-\pi^0$ from the decays $D^0 \rightarrow \pi^+\pi^-\pi^+\pi^-\pi^0\pi^0$ and $D^+ \rightarrow \pi^+\pi^-\pi^+\pi^-\pi^0$ in the K_S^0 or ω signal region may survive in the event selection criteria and form peaking backgrounds around the D mass in the M_{BC}^{sig} distributions. Figures 1(a) and 1(c) also show the used 1D K_S^0 and 2D ω sideband regions, respectively.

In the studies of $D^{0(+)} \rightarrow K_S^0\pi^{0(+)}\omega$, the candidate events lying in the combined 1D K_S^0 sideband and 2D

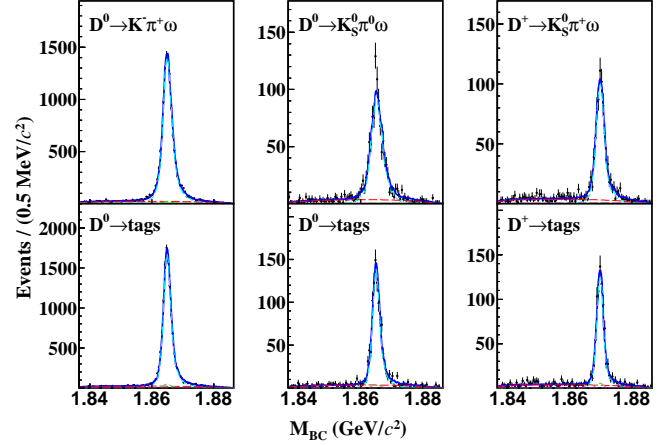


Fig. 4. Projections on M_{BC}^{tag} (bottom) and M_{BC}^{sig} (top) of the 2D fits to the double-tag candidate events for $D^0 \rightarrow K^-\pi^+\omega$, $D^0 \rightarrow K_S^0\pi^0\omega$, and $D^+ \rightarrow K_S^0\pi^+\omega$. The dots with error bars are data. The blue curves are the fit results. The sky blue dashed curves are the fitted signal and the green curves and light green dotted curves are the BKG I, the red curves are the BKG II, the purple curves are the BKG III.

ω signal region, the combined 1D K_S^0 signal and 2D ω sideband region, and the combined 1D K_S^0 sideband and 2D ω sideband region, are called peaking backgrounds A, B, and C, respectively. In the study of $D^0 \rightarrow K^-\pi^+\omega$, the candidate events in the 2D ω sideband region are called peaking background B.

The yields of the peaking backgrounds A/B/C ($N_{\text{sbA/B/C}}$) are obtained by similar 2D fits to the corresponding M_{BC}^{tag} versus M_{BC}^{sig} distributions of the individual candidate events in data. The net double-tag yield ($N_{\text{DT}}^{\text{net}}$) is calculated by

$$N_{\text{DT}}^{\text{net}} = N_{\text{DT}}^{\text{tot}} - f_1 N_{\text{sbA}} - f_2 N_{\text{sbB}} + f_1 f_2 N_{\text{sbC}}. \quad (5)$$

Here f_1 and f_2 are the factors normalizing the background yields in the K_S^0 and ω sideband regions to their corresponding signal regions, respectively. These factors are obtained based on MC simulations. The f_1 values are 0.5 for both $D^0 \rightarrow K_S^0\pi^0\omega$ and $D^+ \rightarrow K_S^0\pi^+\omega$ decays, and it is taken to be 0 in the $D^0 \rightarrow K^-\pi^+\omega$ decay because there is no K_S^0 involved. The f_2 values are 1.44 ± 0.04 , 1.32 ± 0.03 , and 1.28 ± 0.06 for $D^0 \rightarrow K^-\pi^+\omega$, $D^0 \rightarrow K_S^0\pi^0\omega$ and $D^+ \rightarrow K_S^0\pi^+\omega$, respectively, where the uncertainties are mainly due to various sub-resonance components. The values of N_{sbA} , N_{sbB} , N_{sbC} , and $N_{\text{DT}}^{\text{net}}$ are summarized in Table 1.

VI. DETECTION EFFICIENCIES AND BRANCHING FRACTIONS

Figure 5 shows the Dalitz plots of the accepted candidates in data. Figure 6 displays the $M_{K\pi}$, $M_{\pi\omega}$,

and $M_{\bar{K}\omega}$ distributions of $D \rightarrow \bar{K}\pi\omega$ candidate events after requiring $|M_{\text{BC}}^{\text{tag(sig)}} - M_D| < 0.005 \text{ GeV}/c^2$. Signals of $\bar{K}^{*0}(892)$ can be observed in the $M_{\bar{K}\pi}$ spectra for $D^0 \rightarrow K^-(K_S^0)\pi^{+(0)}\omega$ decays. However, no obvious $K^{*+}(892)$ signal is observed in the $M_{\bar{K}\pi}$ spectrum for the $D^+ \rightarrow K^0\pi^+\omega$ decay because the $D^+ \rightarrow K^{*+}(892)\omega$ decay is a doubly Cabibbo-suppressed process. We can see that the distributions of MC simulated events, uniformly generated across the phase space, are not in good agreement with the data distributions. To resolve these disagreements, we modify the MC generator according to the Dalitz plots of $D \rightarrow \bar{K}\pi\omega$ in data, by implementing the same method as used in Ref. [36]. In the Dalitz plot, the signal and background components are modeled by the efficiency-corrected phase space (PHSP) MC simulation and the inclusive MC simulation, respectively. In Fig. 6, we can see that the modified MC distributions agree well with the data distributions. Therefore, we use the modified MC samples to evaluate the detection efficiencies of the signal decays (ϵ_{sig}). The resulting efficiencies are summarized in the seventh column of Table 1.

With the numbers of $N_{\text{ST}}^{\text{tot}}$, $N_{\text{DT}}^{\text{net}}$, and ϵ_{sig} shown in Table 1, the branching fractions of the hadronic decays $D^0 \rightarrow K^-\pi^+\omega$, $D^0 \rightarrow K_S^0\pi^0\omega$, and $D^+ \rightarrow K_S^0\pi^+\omega$ are determined. The resulting branching fractions are summarized in the eighth column of Table 1.

VII. SYSTEMATIC UNCERTAINTIES

In the measurements of the branching fractions ($\mathcal{B}(D^0 \rightarrow K^-\pi^+\omega)$, $\mathcal{B}(D^0 \rightarrow K_S^0\pi^0\omega)$, and $\mathcal{B}(D^+ \rightarrow K_S^0\pi^+\omega)$) and the branching fraction ratios ($\mathcal{R}^0 \equiv \frac{\mathcal{B}(D^0 \rightarrow K_S^0\pi^0\omega)}{\mathcal{B}(D^0 \rightarrow K^-\pi^+\omega)}$ and $\mathcal{R}^+ \equiv \frac{\mathcal{B}(D^+ \rightarrow K_S^0\pi^+\omega)}{\mathcal{B}(D^0 \rightarrow K^-\pi^+\omega)}$), the sources of the systematic uncertainties are summarized in Table 2. Each of them is evaluated relative to the measured branching fraction. See below for details.

- **Single-tag yields:** The uncertainties in the total single-tag \bar{D}^0 and D^- yields were studied in [22–24]. They are 0.5% for both neutral and charged \bar{D} .
- **Tracking (PID) of K^\pm/π^\pm :** The tracking (PID) efficiencies of K^\pm/π^\pm are investigated with double-tag $D\bar{D}$ hadronic events using a partial reconstruction (identification) technique. No significant biases are found. The averaged ratios between data and MC efficiencies ($f_{K \text{ or } \pi}^{\text{tracking(PID)}} = \frac{\epsilon_{K \text{ or } \pi}^{\text{tracking(PID)}}[\text{data}]}{\epsilon_{K \text{ or } \pi}^{\text{tracking(PID)}}[\text{MC}]}$) of tracking (PID) for K^\pm or π^\pm are weighted by the corresponding momentum spectra of signal MC events, giving f_K^{tracking} to be 1.021 and f_π^{tracking} to be close to unity. After correcting the MC efficiencies by f_K^{tracking} , the residual uncertainties of $f_{K \text{ or } \pi}^{\text{tracking}}$ are assigned as the systematic uncertainties of tracking

efficiencies, which are 0.3% per K^\pm and 0.3% per π^\pm . f_K^{PID} and f_π^{PID} are all close to unity and their individual uncertainties, 0.3% are taken as the associated systematic uncertainties per K^\pm or π^\pm .

- **K_S^0 reconstruction:** A control sample of $J/\psi \rightarrow K^*(892)^\mp K^\pm$ and $J/\psi \rightarrow \phi K_S^0 K^\pm \pi^\mp$ was used to evaluate the efficiency of the K_S^0 reconstruction [37]. The efficiency includes effects due to the $\pi^+\pi^-$ track selection, the vertex fit, requirements on the decay length, and the K_S^0 mass window. We take 1.5% per K_S^0 to be the associated systematic uncertainty.
- **π^0 reconstruction:** To study the efficiency of π^0 reconstruction, we used the control sample of the double-tag $D\bar{D}$ hadronic decays $D^0 \rightarrow K^-\pi^+$, $K^-\pi^+\pi^+\pi^-$ versus $\bar{D}^0 \rightarrow K^+\pi^-\pi^0$, $K_S^0\pi^0$ [22, 23]. The efficiency includes effects due to the photon selection, the 1-C kinematic fit, and the π^0 mass window. The data/MC ratio for the π^0 reconstruction efficiency is found to be $(99.1 \pm 0.7)\%$. After correcting the MC signal efficiency by this ratio, a systematic uncertainty of 0.7% is assigned to each π^0 .
- **2D fit on $M_{\text{BC}}^{\text{tag}}$ versus $M_{\text{BC}}^{\text{sig}}$:** To investigate the systematic uncertainty due to the 2D fit on $M_{\text{BC}}^{\text{tag}}$ versus $M_{\text{BC}}^{\text{sig}}$, we remeasure the branching fraction by using alternative signal shapes with different MC matching requirements, and alternative end-points of the ARGUS function $E_b \pm 0.2 \text{ MeV}/c^2$. For each source, the largest changes to the nominal branching fractions are taken as its systematic uncertainty. Quadratically summing over these two effects, we assign the systematic uncertainties in the 2D fit to be 0.3%, 1.2%, and 2.1% for $D^0 \rightarrow K^-\pi^+\omega$, $D^0 \rightarrow K_S^0\pi^0\omega$, and $D^+ \rightarrow K_S^0\pi^+\omega$, respectively.
- **ΔE_{sig} requirement:** The systematic uncertainty due to the ΔE_{sig} requirement is assigned to be 0.3%, 0.4%, and 0.4% for $D^0 \rightarrow K^-\pi^+\omega$, $D^0 \rightarrow K_S^0\pi^0\omega$, and $D^+ \rightarrow K_S^0\pi^+\omega$, respectively, which corresponds to the largest efficiency difference with and without smearing the data-MC Gaussian resolution of ΔE_{sig} for signal MC events. Here, the smeared Gaussian parameters are obtained by using the samples of double-tag events $D^0 \rightarrow K^-\pi^+$, $D^0 \rightarrow K^-\pi^+\pi^0$, $D^0 \rightarrow K^-\pi^+\pi^0\pi^0$, $D^+ \rightarrow K_S^0\pi^+$ and $D^+ \rightarrow K^-\pi^+\pi^+\pi^0$ versus the same \bar{D} tags in our nominal analysis.
- **MC modeling:** To estimate the systematic uncertainty in the MC modeling, we vary the bin sizes and the MC-simulated background sizes of the input $M_{\bar{K}\pi}^2$ versus $M_{\pi\omega}^2$ distributions in the generator by one quarter. The largest changes to the nominal detection efficiencies, 0.6%, 1.2%, and 2.1%, are taken as the homologous systematic

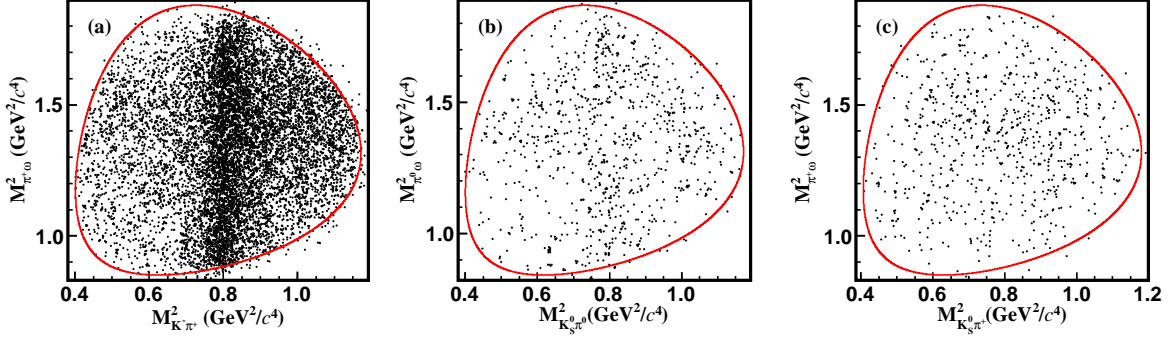


Fig. 5. Dalitz plots of the accepted DT candidates for (a) $D^0 \rightarrow K^-\pi^+\omega$, (b) $D^0 \rightarrow K_S^0\pi^0\omega$, and (c) $D^+ \rightarrow K_S^0\pi^+\omega$. The red curves show the kinematically allowed regions.

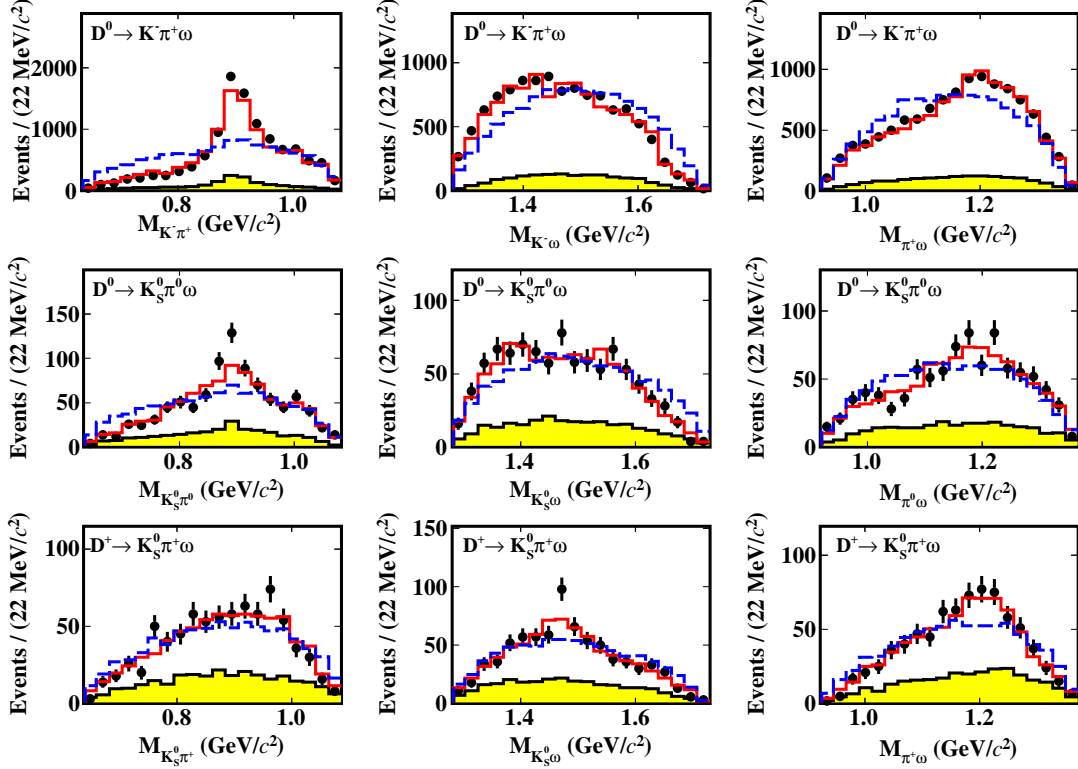


Fig. 6. The $M_{\bar{K}\pi}$, $M_{\pi\omega}$, and $M_{\bar{K}\omega}$ distributions of the $D \rightarrow \bar{K}\pi\omega$ candidate events in the mass windows of $|M_{\text{BC}}^{\text{tag(sig)}} - M_D| < 0.005 \text{ GeV}/c^2$. Data are shown as points with error bars; the blue dashed and red solid histograms are the PHSP MC and modified MC samples, respectively; the yellow shaded histograms are the simulated backgrounds estimated from the inclusive MC sample.

uncertainties for $D^0 \rightarrow K^-\pi^+\omega$, $D^0 \rightarrow K_S^0\pi^0\omega$, and $D^+ \rightarrow K_S^0\pi^+\omega$, respectively.

- **MC statistics:** The uncertainties due to MC statistics are considered as a source of systematic uncertainties, which are 0.4%, 0.7%, and 0.6% for $D^0 \rightarrow K^-\pi^+\omega$, $D^0 \rightarrow K_S^0\pi^0\omega$, and $D^+ \rightarrow K_S^0\pi^+\omega$, respectively.

- **Quoted branching fractions:** The uncertainties of the quoted branching fractions of $K_S^0 \rightarrow \pi^+\pi^-$, $\omega \rightarrow \pi^+\pi^-\pi^0$, and $\pi^0 \rightarrow \gamma\gamma$ are also considered as a source of systematic uncertainties, which are 0.07, 0.8%, and 0.03% [3], respectively.
- **Quantum correlation effect:** The measurement of the branching fraction of the neutral D decay

Table 1. The double-tag yields in data ($N_{\text{DT}}^{\text{tot}}$), the yields of peaking backgrounds A/B/C ($N_{\text{sbA/B/C}}$), the net double-tag yields in data ($N_{\text{DT}}^{\text{net}}$), the signal efficiencies (ϵ_{sig}), the branching fractions (\mathcal{B}_{sig}) and the comparisons to world averages (\mathcal{B}_{PDG}). The efficiencies include the branching fractions of $K_S^0 \rightarrow \pi^+\pi^-$, $\omega \rightarrow \pi^+\pi^-\pi^0$, and $\pi^0 \rightarrow \gamma\gamma$. The uncertainties of $N_{\text{DT}}^{\text{tot}}$ and ϵ_{sig} are statistical only, the first and second uncertainties of \mathcal{B}_{sig} are statistical and systematic, respectively.

Decay mode	$N_{\text{DT}}^{\text{tot}}$	N_{sbA}	N_{sbB}	N_{sbC}	$N_{\text{DT}}^{\text{net}}$	$\epsilon_{\text{sig}} (\%)$	$\mathcal{B}_{\text{sig}} (\%)$	$\mathcal{B}_{\text{PDG}} (\%)$
$D^0 \rightarrow K^-\pi^+\omega$	11745 ± 115	...	1092 ± 38	...	10174 ± 128	12.96 ± 0.06	$3.392 \pm 0.044 \pm 0.085$	3.0 ± 0.6
$D^0 \rightarrow K_S^0\pi^0\omega$	944 ± 33	27 ± 6	70 ± 10	190 ± 14	697 ± 41	3.43 ± 0.04	$0.848 \pm 0.046 \pm 0.031$	N/A
$D^+ \rightarrow K_S^0\pi^+\omega$	770 ± 30	28 ± 6	67 ± 10	130 ± 13	523 ± 35	5.35 ± 0.04	$0.707 \pm 0.041 \pm 0.029$	N/A

Table 2. Relative systematic uncertainties (in %) in the determinations of $\mathcal{B}(D^0 \rightarrow K^-\pi^+\omega)$, $\mathcal{B}(D^0 \rightarrow K_S^0\pi^0\omega)$, $\mathcal{B}(D^+ \rightarrow K_S^0\pi^+\omega)$, \mathcal{R}^0 , and \mathcal{R}^+ . For the last two columns, the numbers before and after ‘/’ are the uncanceled systematic uncertainties of $\mathcal{B}(D^0 \rightarrow K^-\pi^+\omega)$ and $\mathcal{B}(D^{0(+)} \rightarrow K_S^0\pi^{0(+)}\omega)$ in calculating \mathcal{R}^0 and \mathcal{R}^+ .

Source	$\mathcal{B}(D^0 \rightarrow K^-\pi^+\omega)$	$\mathcal{B}(D^0 \rightarrow K_S^0\pi^0\omega)$	$\mathcal{B}(D^+ \rightarrow K_S^0\pi^+\omega)$	\mathcal{R}^0	\mathcal{R}^+
Single-tag yields	0.5	0.5	0.5	–	0.7
Tracking of K^\pm	0.3	–	–	0.3	0.3
Tracking of π^\pm	0.9	0.6	0.9	0.3	–
PID of K^\pm	0.3	–	–	0.3	0.3
PID of π^\pm	0.9	0.6	0.9	0.3	–
K_S^0 reconstruction	–	1.5	1.5	1.5	1.5
π^0 reconstruction	0.7	1.4	0.7	0.7	–
2D M_{BC} fit	0.5	1.5	1.8	1.6	1.9
ΔE requirement	0.3	0.4	0.4	0.5	0.5
MC modeling	0.6	1.2	2.1	2.2	1.3
MC statistics	0.4	0.7	0.6	0.8	0.7
Quoted branching fractions	0.8	0.8	0.8	0.1	0.1
Quantum correlation effect	0.6	0.4	–	0.7	0.6
K_S^0 sideband	–	0.1	0.4	0.1	0.4
ω sideband	1.2	1.0	1.3	1.6	1.8
Rejection of $D \rightarrow \bar{K}\pi\eta$	0.5	1.2	0.3	1.3	0.6
The factor of f^ω	0.3	0.7	1.0	–	–
Total	2.5	3.7	4.1	4.0	3.8

is affected by the quantum correlation effect. For the decay $D^0 \rightarrow K_S^0\pi^0\omega$ the CP -even component is estimated by the CP -even tag $D^0 \rightarrow K^+K^-$ and the CP -odd tag $D^0 \rightarrow K_S^0\pi^0$. Using the same method as described in Ref. [38] and the necessary parameters quoted from Refs. [39–41], the correction factor to account for the quantum correlation effect on the measured branching fraction is found to be $(96.1 \pm 0.4_{\text{stat}})\%$. After correcting the signal efficiency by this factor, the residual error, 0.4%, is assigned as the associated systematic uncertainty. The associated uncertainty in the measurement of the branching fraction of $D^0 \rightarrow K^-\pi^+\omega$ is assigned to be 0.6% by the method discussed in Ref. [42], and it is controlled by the ratio of Cabibbo-suppressed and Cabibbo-favored rate combined with the strong phase difference between two amplitudes.

- **K_S^0 sideband, ω sideband, and rejection of $D \rightarrow \bar{K}\pi\eta$:** The uncertainties due to the

choices of the K_S^0 and ω sideband regions (the rejection requirement of $D \rightarrow \bar{K}\pi\eta$) are studied by shifting the nominal regions (requirement) by ± 0.005 (0.010) GeV/c^2 . For each source, the largest difference of the branching fraction is taken as the corresponding systematic uncertainty for each signal decay.

- **The factor of f^ω :** The systematic uncertainty due to the factor f^ω is assigned by examining the changes of branching fractions via varying the factors by $\pm 1\sigma$. They are assigned as 0.3%, 0.7% and 1.0% for $D^0 \rightarrow K^-\pi^+\omega$, $D^0 \rightarrow K_S^0\pi^0\omega$ and $D^+ \rightarrow K_S^0\pi^+\omega$, respectively.

Adding these systematic uncertainties in quadrature, we obtain the total systematic uncertainties for the measurements of $\mathcal{B}(D^0 \rightarrow K^-\pi^+\omega)$, $\mathcal{B}(D^0 \rightarrow K_S^0\pi^0\omega)$, $\mathcal{B}(D^+ \rightarrow K_S^0\pi^+\omega)$, \mathcal{R}^0 , and \mathcal{R}^+ to be 2.5%, 3.7%, 4.1%, 4.0%, and 3.8%, respectively.

VIII. SUMMARY

With a data sample corresponding to an integrated luminosity of 2.93 fb^{-1} , taken with the BESIII [43] detector at $\sqrt{s} = 3.773\text{ GeV}$, we measure the absolute branching fractions of $D^0 \rightarrow K^-\pi^+\omega$, $D^0 \rightarrow K_S^0\pi^0\omega$, and $D^+ \rightarrow K_S^0\pi^+\omega$. The branching fractions of $D^0 \rightarrow K_S^0\pi^0\omega$ and $D^+ \rightarrow K_S^0\pi^+\omega$ are measured for the first time. Our result of the branching fraction of $D^0 \rightarrow K^-\pi^+\omega$ is consistent with the previous result within uncertainties, but the accuracy is improved by a factor of seven. The comparisons of measurements and the world-average values are shown in Table 1. Using the branching fractions measured in this work, we determine the branching fraction ratios to be $\mathcal{R}^0 \equiv \frac{\mathcal{B}(D^0 \rightarrow K_S^0\pi^0\omega)}{\mathcal{B}(D^0 \rightarrow K^-\pi^+\omega)} = 0.23 \pm 0.01_{\text{stat}} \pm 0.01_{\text{syst}}$ and $\mathcal{R}^+ \equiv \frac{\mathcal{B}(D^+ \rightarrow K_S^0\pi^+\omega)}{\mathcal{B}(D^0 \rightarrow K^-\pi^+\omega)} = 0.21 \pm 0.01_{\text{stat}} \pm 0.01_{\text{syst}}$. Both \mathcal{R}^0 and \mathcal{R}^+ significantly deviate from their expected values of the SIM. These deviations may arise from a possible strong phase difference between two decay amplitudes due to final state interactions [5, 6].

IX. ACKNOWLEDGEMENTS

The BESIII collaboration thanks the staff of BEPCII and the IHEP computing center for their strong support. This work is supported in part by National Key Research

and Development Program of China under Contracts Nos. 2020YFA0406400, 2020YFA0406300; National Natural Science Foundation of China (NSFC) under Contracts Nos. 11625523, 11635010, 11775230, 11735014, 11822506, 11835012, 11935015, 11935016, 11935018, 11961141012; the Chinese Academy of Sciences (CAS) Large-Scale Scientific Facility Program; Joint Large-Scale Scientific Facility Funds of the NSFC and CAS under Contracts Nos. U1732263, U1832207, U1632109; CAS Key Research Program of Frontier Sciences under Contracts Nos. QYZDJ-SSW-SLH003, QYZDJ-SSW-SLH040; 100 Talents Program of CAS; INPAC and Shanghai Key Laboratory for Particle Physics and Cosmology; ERC under Contract No. 758462; European Union Horizon 2020 research and innovation programme under Contract No. Marie Skłodowska-Curie grant agreement No 894790; German Research Foundation DFG under Contracts Nos. 443159800, Collaborative Research Center CRC 1044, FOR 2359, FOR 2359, GRK 214; Istituto Nazionale di Fisica Nucleare, Italy; Ministry of Development of Turkey under Contract No. DPT2006K-120470; National Science and Technology fund; Olle Engkvist Foundation under Contract No. 200-0605; STFC (United Kingdom); The Knut and Alice Wallenberg Foundation (Sweden) under Contract No. 2016.0157; The Royal Society, UK under Contracts Nos. DH140054, DH160214; The Swedish Research Council; U. S. Department of Energy under Contracts Nos. DE-FG02-05ER41374, DE-SC-0012069.

-
- [1] D. M. Asner *et al.*, *Int. J. Mod. Phys. A* **24**, S1-794 (2009).
 - [2] M. Saur and F. S. Yu, *Sci. Bull.* **65**, 1428-1431 (2020).
 - [3] P. A. Zyla *et al.* (Particle Data Group), *Prog. Theor. Exp. Phys.* **2020**, 083C01 (2020).
 - [4] H. Albrecht *et al.* (ARGUS Collaboration), *Z. Phys. C* **56**, 7 (1992).
 - [5] M. Peshkin and J. L. Rosner, *Nucl. Phys. B* **122**, 144 (1977).
 - [6] M. Gronau and J. L. Rosner, *Phys. Rev. D* **79**, 074022 (2009).
 - [7] R. Aaij *et al.* (LHCb Collaboration), *Synergy of BESIII and LHCb physics programmes*, LHCb-PUB-2016-025.
 - [8] R. Aaij *et al.* (LHCb Collaboration), *Phys. Lett. B* **757**, 558 (2016).
 - [9] J. P. Lee *et al.* (BaBar Collaboration), *Phys. Rev. Lett.* **122**, 081802 (2019).
 - [10] M. Ablikim *et al.* (BESIII Collaboration), *Phys. Rev. D* **97**, 072015 (2018).
 - [11] M. Ablikim *et al.* (BESIII Collaboration), *Chin. Phys. C* **37**, 123001 (2013); *Phys. Lett. B* **753**, 629 (2016).
 - [12] M. Ablikim *et al.* (BESIII Collaboration), *Nucl. Instrum. Meth. A* **614**, 345 (2010).
 - [13] C. H. Yu *et al.*, *Proceedings of IPAC2016*, Busan, Korea, 2016.
 - [14] M. Ablikim *et al.* (BESIII Collaboration), *Chin. Phys. C* **45**, 023002(2021).
 - [15] K. Zhu *et al.* *Chin. Phys. C* **34**, 1779-1784(2010).
 - [16] S. Agostinelli *et al.* (GEANT4 Collaboration), *Nucl. Instrum. Meth. A* **506**, 250 (2003).
 - [17] S. Jadach, B. F. L. Ward, and Z. Was, *Comp. Phys. Commu.* **130**, 260 (2000); *Phys. Rev. D* **63**, 113009 (2001).
 - [18] D. J. Lange, *Nucl. Instrum. Meth. A* **462**, 152 (2001); R. G. Ping, *Chin. Phys. C* **32**, 599 (2008).
 - [19] J. C. Chen, G. S. Huang, X. R. Qi, D. H. Zhang, and Y. S. Zhu, *Phys. Rev. D* **62**, 034003 (2000).
 - [20] E. Richter-Was, *Phys. Lett. B* **303**, 163 (1993).
 - [21] H. B. Li and X. R. Lyu, *arXiv:2103.00908 [hep-ex]*.
 - [22] M. Ablikim *et al.* (BESIII Collaboration), *Eur. Phys. J. C* **76**, 369 (2016).
 - [23] M. Ablikim *et al.* (BESIII Collaboration), *Chin. Phys. C* **40**, 113001 (2016).
 - [24] M. Ablikim *et al.* (BESIII Collaboration), *Phys. Rev. Lett.* **121**, 171803 (2018).
 - [25] M. Ablikim *et al.* (BESIII Collaboration), *Phys. Rev. Lett.* **123**, 231801 (2019).
 - [26] M. Ablikim *et al.* (BESIII Collaboration), *Phys. Rev. D* **101**, 052009 (2020).
 - [27] M. Ablikim *et al.* (BESIII Collaboration), *Phys. Rev. D* **101**, 072005 (2020).
 - [28] M. Ablikim *et al.* (BESIII Collaboration), *Phys. Rev. D* **102**, 052006 (2020).

- [29] M. Ablikim *et al.* (BESIII Collaboration), *Phys. Rev. Lett.* **124**, 231801 (2020).
- [30] M. Ablikim *et al.* (BESIII Collaboration), *Phys. Rev. Lett.* **124**, 241803 (2020).
- [31] M. Ablikim *et al.* (BESIII Collaboration), *Phys. Rev. Lett.* **125**, 141802 (2020).
- [32] M. Ablikim *et al.* (BESIII Collaboration), *Phys. Rev. D.* **102**, 112005 (2020).
- [33] M. Ablikim *et al.* (BESIII Collaboration), *Phys. Lett. B* **734**, 227 (2014).
- [34] H. Albrecht *et al.* (ARGUS Collaboration), *Phys. Lett. B* **241**, 278 (1990).
- [35] S. Dobbs *et al.* (CLEO Collaboration), *Phys. Rev. D.* **76**, 112001 (2007).
- [36] M. Ablikim *et al.* (BESIII Collaboration), *Phys. Rev. D.* **98**, 092009 (2018).
- [37] M. Ablikim *et al.* (BESIII Collaboration), *Phys. Rev. D* **92**, 112008 (2015).
- [38] M. Ablikim *et al.* (BESIII Collaboration), *Phys. Rev. D* **100**, 072006 (2019).
- [39] T. Gershon, J. Libby, and G. Wilkinson, *Phys. Lett. B* **750**, 338 (2015).
- [40] T. Evans *et al.*, *Phys. Lett. B* **757**, 520 (2016); **765**, 402(E) (2017).
- [41] Heavy Flavor Averaging Group (HFLAV), (<http://www.slac.stanford.edu/xorg/hflav/charm/>).
- [42] S. Dobbs *et al.* (CLEO Collaboration), *Phys. Rev. D* **76** 112001 (2007) .
- [43] M. Ablikim *et al.* (BESIII Collaboration), *Chin. Phys. C* **44**, 040001 (2020).